J Mol Model
DOI 10.1007/s00894-012-1554-5

ORIGINAL PAPER

Prodrugs of fumarate esters for the treatment of psoriasis and multiple sclerosis—a computational approach

Rafik Karaman · Ghadeer Dokmak · Maryam Bader · Hussein Hallak · Mustafa Khamis · Laura Scrano · Sabino Aurelio Bufo

Received: 12 May 2012 / Accepted: 30 July 2012

Abstract Density functional theory (DFT) calculations at B3LYP/6-31 G (d,p) and B3LYP/6-311+G(d,p) levels for the substituted pyridine-catalyzed isomerization of monomethyl maleate revealed that isomerization proceeds via four steps, with the rate-limiting step being proton transfer from the substituted pyridinium ion to the C=C double bond in INT1. In addition, it was found that the isomerization rate (maleate to fumarate) is solvent dependent. Polar solvents, such as water, tend to accelerate the isomerization rate, whereas apolar solvents, such as chloroform, act to slow down the reaction. A linear correlation was obtained between the isomerization activation energy and the dielectric constant of the solvent. Furthermore, linearity was achieved when the activation energy was plotted against the pK_a value of the catalyst. Substituted-pyridine derivatives with high pK_a values were able to catalyze isomerization more efficiently than those with low pK_a values. The calculated relative rates for prodrugs **1**–**6** were: **1** (406.7), **2** (7.6×10^6), **3** (1.0), **4** (20.7), **5** (13.5) and **6** (2.2×10^3). This result indicates that isomerizations of prodrugs **1** and **3**–**5** are expected to be slow and that of prodrugs **2** and **6** are expected to be relatively fast. Hence, prodrugs **2** and **3**–**5** have the potential to be utilized as prodrugs for the slow release of monomethylfumarate in the treatment of psoriasis and multiple sclerosis.

Keywords Prodrug · Psoriasis · Multiple sclerosis · Monomethylmaleate · Isomerization of monomethylmaleate · DFT calculation · Pyridine-catalyzed cis-trans isomerization

Introduction

Fumaric acid esters are chemical compounds derived from the unsaturated dicarbonic acid, fumaric acid, which is a naturally occurring substance, and is used by cells to produce energy from food. Human skin naturally produces fumaric acid when exposed to sunlight. Fumaric acid is absorbed poorly and cannot be expected to have any pharmacologic effect following oral administration. However, esters of fumaric acid, such as monoethylfumarate, monomethylfumarate, diethylfumarate and dimethylfumarate, are potent chemicals and have been used in the treatment of psoriasis in European countries for over three decades [1]. The use of fumaric acid esters in oral preparations, and topically for the treatment of psoriasis, was first introduced in 1959 by the German chemist Schweckendiek [2]. In 1994, Fumaderm, an enteric-coated tablet containing dimethylfumarate and calcium, magnesium and zinc salts of monoethylfumarate was approved in Germany for the treatment of psoriasis and since then has become the systemic therapy most commonly used in that country [3]. Dimethylfumarate is metabolized rapidly to monomethyl fumarate, which, together with dimethylfumarate, is regarded as the main active metabolite. Treatment with dimethylfumarate and/or monomethylfumarate produces a beneficial shift towards Th2-like cytokine secretion associated with a

Electronic supplementary material The online version of this article (doi:10.1007/s00894-012-1554-5) contains supplementary material, which is available to authorized users.

R. Karaman (✉) · G. Dokmak · M. Bader · H. Hallak
Department of Bioorganic Chemistry, Faculty of Pharmacy,
Al-Quds University,
PO Box 20002, Jerusalem, Israel
e-mail: dr_karaman@yahoo.com

M. Khamis
Department of Chemistry and Chemical Technology,
College of Science and Technology, Al-Quds University,
Jerusalem, Israel

L. Scrano · S. A. Bufo
Department of Agriculture, Forestry and Environment,
University of Basilicata,
Potenza 85100, Italy

Published online: 02 September 2012

reduction in peripheral lymphocytes (primarily T cells) and inhibits the proliferation of epidermal keratinocytes in patients with psoriasis [4]. Little is known about the pharmacokinetics of fumarate esters. Recent data from in vitro experiments suggest that hydrolysis of dimethylfumarate to the bioactive metabolite monomethylfumarate occurs rapidly at pH 8, a value usually arising in small intestine environments, but not at pH 1, which is found typically in the stomach [5]. This finding let us conceptualize that hydrolysis of dimethylfumarate occurs mainly in the small intestine, and that monomethylfumarate and monoethylfumarate can be absorbed into the blood circulation where they interact with blood cells.

Monomethylfumarate and monoethylfumarate may also influence inflammatory cells in psoriatic lesions. In humans, serum concentrations of monomethylfumarate after oral intake reach peak levels within 5–6 h [6]. Brain inflammation plays a central role in multiple sclerosis (MS). One of the disadvantages of currently available disease-modifying drugs for multiple sclerosis is their parenteral administration. Moreover, efficacy is only partial. Most patients treated with first-line disease-modifying drugs do not remain relapse-free. There is a need for new oral drugs that are more effective than currently available compounds. Some innovative oral drugs with new mechanisms of action recently showed promising results in clinical trials. One of these emerging drugs is BG-12 —a fumaric acid ester. Its active agent, dimethyl fumarate, was first included in fumaric acid ester treatments for psoriasis as mentioned above [3, 4, 6].

Common adverse events associated with fumaric acid ester therapy are gastrointestinal complaints and flushing [3]. Gastrointestinal adverse events, such as diarrhea, mild stomach upsets, stomach cramps, fullness and flatulence, occur in more than two-thirds of patients and are reported most frequently between 4 and 12 weeks of treatment [3, 6]. Flushing occurs mostly at the onset of treatment and becomes less frequent with further exposure [3]. Dose reduction of fumaric acid esters may also be used to manage symptoms; however, discontinuation should be considered in persistent cases [6]. Gastrointestinal adverse events and flushing together lead to discontinuation of fumaric acid esters therapy in approximately 7 % of patients [3]. Overall, the rate of discontinuation due to adverse events and/or noncompliance with treatment is 30–40 % [7]. Other challenges for fumeric acid esters include the inconvenience of taking up to three daily doses and the requirement for frequent laboratory monitoring.

Continuing our studies on the design and synthesis of prodrugs for certain drugs that have poor bioavailability or/and side effects, we sought to investigate the pyridine-catalyzed isomerization of monomethyl maleate (cis isomer lacking biological activity) into its trans isomer, monomethylfumarate (trans isomer having biological activity) in order to utilize the former as a prodrug for the latter [8–13]. Unraveling the mechanism of this cis-trans isomerization might shed light on the kinetics of this conversion and might lead to a potential prodrug system capable of delivering the parental drug in a controlled release manner with higher bioavailability and less side effects than the current direct administration of monomethyl, monoethyl fumarates or dimethyl fumarate.

The isomerization of maleates to fumarates is catalyzed by a variety of reagents. The cis-trans isomerization is possible via photolysis in the presence of a catalytic amount of bromine. Light converts bromine into a bromine radical, which allows a single bond rotation after its addition to the C–C double bond of the maleate moeity. Isomerization of maleates into fumarates can be achieved by the addition of mineral acid. Reversible addition of proton leads to free rotation about the central C–C bond and formation of the more stable isomer, fumarate. [14–18]. Amine-catalyzed cis-trans isomerization has been known for more than seven decades [14, 15]. Cis–trans isomerization catalyzed by nucleophiles has been reported in the case of dialkyl maleate and fumarate. It has been documented that ammonia, primary amines and secondary amines catalyze readily the isomerization of dialkyl maleate into the corresponding fumarate ester. However, this isomerization is not catalyzed by tertiary amines due to the lack of a proton [14, 15]. Dimethyl maleate is converted into dimethyl fumarate using aminal as a catalyst [19]. Further, it was also documented that NBS-(N-bromosuccinimide) bromination conditions were sufficient for *Z* to *E* alkene isomerization. Upon treatment with NBS-AIBN (N-bromosuccinimide dibenzoyl peroxide-azobisisobutyronitrile), dimethyl maleate gave dimethyl fumarate in very high yield. Isomerization of the C–C double bond took place via in situ addition–elimination of the bromine radical [17]. Cis-trans isomerization of dimethyl maleate to dimethyl fumarate by the addition of a protic imidazolium species was also reported. The mechanism suggested relies on addition of the protic imidazolium moiety to the C–C double bond, which allows rotation and subsequent imidazolium elimination [20].

Another approach to improving the physicochemical properties of pharmaceuticals is co-crystallization of solid forms of the active ingredients. Other solid forms, including polymorphs, solvates, and salts, can be chosen to optimize the physical properties of active ingredients. For example, the dissolution rate of the α-polymorph of chloramphenicol palmitate is quite different from that of its β-polymorph. Hence, the bioavailability of the two different polymorphs is different. Other examples are theophylline and erythromycin, the hydrate forms of which have different dissolution rates and bioavailability when compared to their anhydrous forms [21–25]. Rao and coworkers examined the structures of the adducts obtained from the cocrystallization of maleic acid with 4,4′-bipyridine, in different solvents. Co-crystallization of maleic acid and 4,4′-bipyridine was obtained when

the solvent used was apolar (e.g., chloroform) but co-crystallization in aprotic polar solvents such as dimethylsulfoxide (DMSO) gave an adduct where maleic acid had isomerized to fumaric acid [26]. Recently, Tocher and coworkers used X-ray diffraction to investigate the two-component crystals formed from pyridine or 4-dimethylaminopyridine with maleic, fumaric, phthalic, isophthalic, or terephthalic acids. Their study revealed that the two-component solid forms involving pyridine included both salts and co-crystals, while 4-dimethylaminopyridine crystallized exclusively as a salt, in agreement with the observed differences in pK_a values. In addition, they reported an in-situ base catalyzed isomerization of maleic acid in co-crystallization experiments involving pyridine [27].

We learned from our recent study on intramolecularity that it is crucial to investigate the reaction mechanism in order to assign factors affecting the reaction rate. This allows better design of an efficient chemical device to be used as a prodrug as well as the potential to chemically release the active ingredient in a controlled (programmable) fashion. For example, we have studied the mechanism of proton transfer in Kirby's enzyme model [28–43] and, based on the results obtained, we designed prodrugs of aza-nucleosides for the treatment of myelodysplastic syndromes where the prodrug linker (Kirby's acetal) is attached to the hydroxyl group of the nucleoside [9]. Furthermore, prodrugs of paracetamol capable of masking its bitterness were also designed such that the linker was covalently linked to the paracetamol phenolic group, which is believed to be the moiety responsible for the bitter taste of the drug [11]. The prodrugs were designed such that they will cleave in physiological environments such as stomach at pH 1.5, intestine at pH 6.5 or/and blood circulation at pH 7.4, with rates that are dependent solely on the structural features of the pharmacologically inactive linker. Different linkers were also investigated for the design of a large number of prodrugs such as anti-Parkinson (dopamine), anti-viral (acyclovir) and anti-malarial (atovaquone) that might be efficient in releasing the parental drugs in various rates that are dependent on the nature or the structural features of the linkers and provide new novel prodrugs that have the potential to have better dissolution and membrane penetration and hence enhanced bioavailability [8–12].

To expand our approach for utilizing intramolecularity in the design of potential fumarates prodrugs, we have studied the mechanism and driving force(s) determining the rate of the substituted pyridine-catalyzed isomerization of monoalkylmaleates. This work was done with the hope that such prodrugs might have the potential to deliver the corresponding fumarates in a controlled release manner, and hence reduce the side effects related to high doses of the corresponding active ingredient, monomethyl or monoethylfumarates.

Based on density functional theory (DFT) calculation results on the pyridine-catalyzed isomerization of **1**–**6** reported herein, six fumarate prodrugs are proposed (Scheme 1). It should be emphasized that the hydrophilic-lipophylic balance value of the prodrug moiety will be dependent on the pH of the target physiologic environment. In the stomach, it is expected that prodrugs **ProD 1** – **6** will be in the carboxylic acid form (a relatively high lipophilicity), whereas in the blood circulation system the carboxylate anion form (a relatively low lipophilicity) will be predominant.

In this paper, we report a DFT computational study on the substituted-pyridine-catalyzed isomerization of **1**–**6** (Scheme 1). Based on the calculated rates for the conversion of **ProD 1**–**6** to the parental drug, monomethylmaleate potential effective prodrugs will be synthesized and tested.

The aims of this work were: (1) to study the mechanistic behavior of substituted pyridine-catalyzed isomerization of monomethylmaleate using six pyridine derivatives as a catalyst and unravel the nature of the force(s) affecting the rate as a function of the substitution on the pyridine ring; and (2) to design various fumarate prodrugs that have the capability to undergo isomerization in physiological environments to provide fumarate in a programmable fashion.

Calculation methods

The Becke three-parameter, hybrid functional [44] combined with the Lee, Yang, and Parr correlation functional [45], denoted B3LYP [46], were employed in DFT calculations. All calculations were carried out using the quantum chemical package Gaussian-2009 [47]. Calculations were carried out based on the restricted Hartree-Fock (HF) method [47]. The starting geometries of all calculated molecules were obtained using the Argus Lab program [48] and were optimized initially at the HF/6-31 G level of theory followed by optimization at the B3LYP/6-31 G(d,p) and B3LYP/6-311+ G(d,p). Second derivatives were estimated for all three N-6 geometrical parameters during optimization. An energy minimum (a stable compound or a reactive intermediate) has no negative vibrational force constant. A transition state is a saddle point with only one negative vibrational force constant [49]. Transition states were located first by the normal reaction coordinate method [50] where enthalpy changes were monitored by stepwise changing of the interatomic distance between two specific atoms. The geometry at the highest point on the energy profile was re-optimized using the energy gradient method at the B3LYP/6-31 G(d,p) and B3LYP/6-311+ G(d,p) levels of theory [47]. The "reaction coordinate method" [50] was used to calculate the activation energy of monomethylmaleate in the presence of a pyridine derivative (Scheme 1). In this method, one bond length was constrained for the appropriate degree of freedom while all other variables were freely optimized. The activation energy values for the first step in the process (proton transfer

Scheme 1 Equilibrium reaction of monomethylmaleate with pyridine derivatives (**1**–**6**)

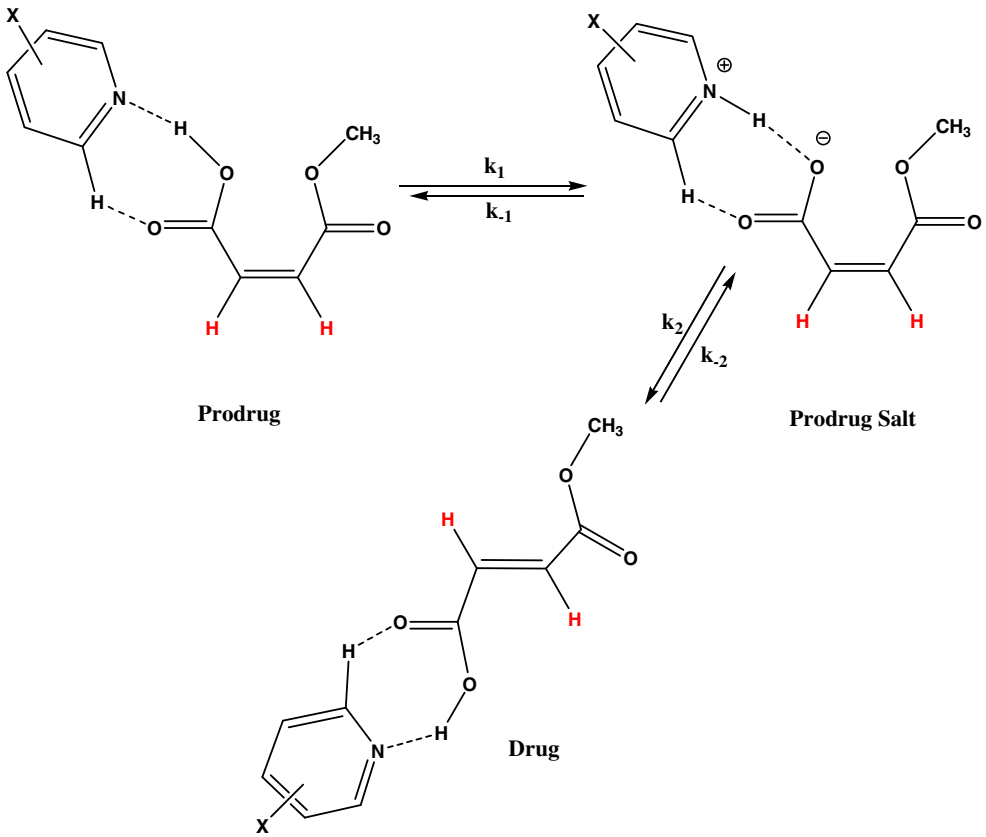

1: X = H
2: X = N(CH$_3$)$_2$
3: X = o-Cl
4: X = m-Cl
5: X = o-F
6: X = o-Me

from the carboxylic group of monomethylmaleate onto the pyridine derivative nitrogen (Scheme 2) were calculated from the difference in energies of the global minimum structures (GM) and the derived transition states (TS_1 in Scheme 2). Similarly, the activation energies for step 2, a proton transfer from the pyridinium derivative cations to the C–C double bond to form INT2 were calculated from the difference in energies of the global minimum structures (GM) and the corresponding TS (TS_2 in Scheme 2). The activation energy values for step 3, an abstraction of a proton from INT3 by a pyridine derivative molecule were calculated from the difference in energies of the GM and the corresponding TS (TS_3 in Scheme 2). The activation energy values for step 4 (proton transfer from a pyridinium derivative cation to the carboxylate anion (step 4 in Scheme 2) were calculated from the difference in energies of the GM structures and the corresponding TS (TS_4 in Scheme 2). Verification of the desired reactants and products was accomplished using the "intrinsic coordinate method" [50]. The TS structures were verified by their single negative frequency. Full optimization of the TSs was accomplished after removing any constraints imposed while executing the energy profile. The activation energies obtained from the DFT at B3LYP/6-31 G (d,p) and B3LYP/6-311+ G(d, p) levels of theory for monomethylmaleate in the presence of pyridine derivatives were calculated with and without the inclusion of solvent (water, chloroform, dimethylsulfoxide, methanol and acetone). Calculations incorporating a solvent were performed using the integral equation formalism model of the polarizable continuum model (PCM) [51–54]. In this model, the cavity is created via a series of overlapping spheres. The radii type employed was the United Atom Topological Model on radii optimized for the PBE0/6-31 G (d) level of theory.

Results and discussion

General considerations

Because the free energy of a carboxylic acid is affected strongly by its conformation, especially when engaging in inter- or intra-molecular hydrogen bonding, we were concerned with

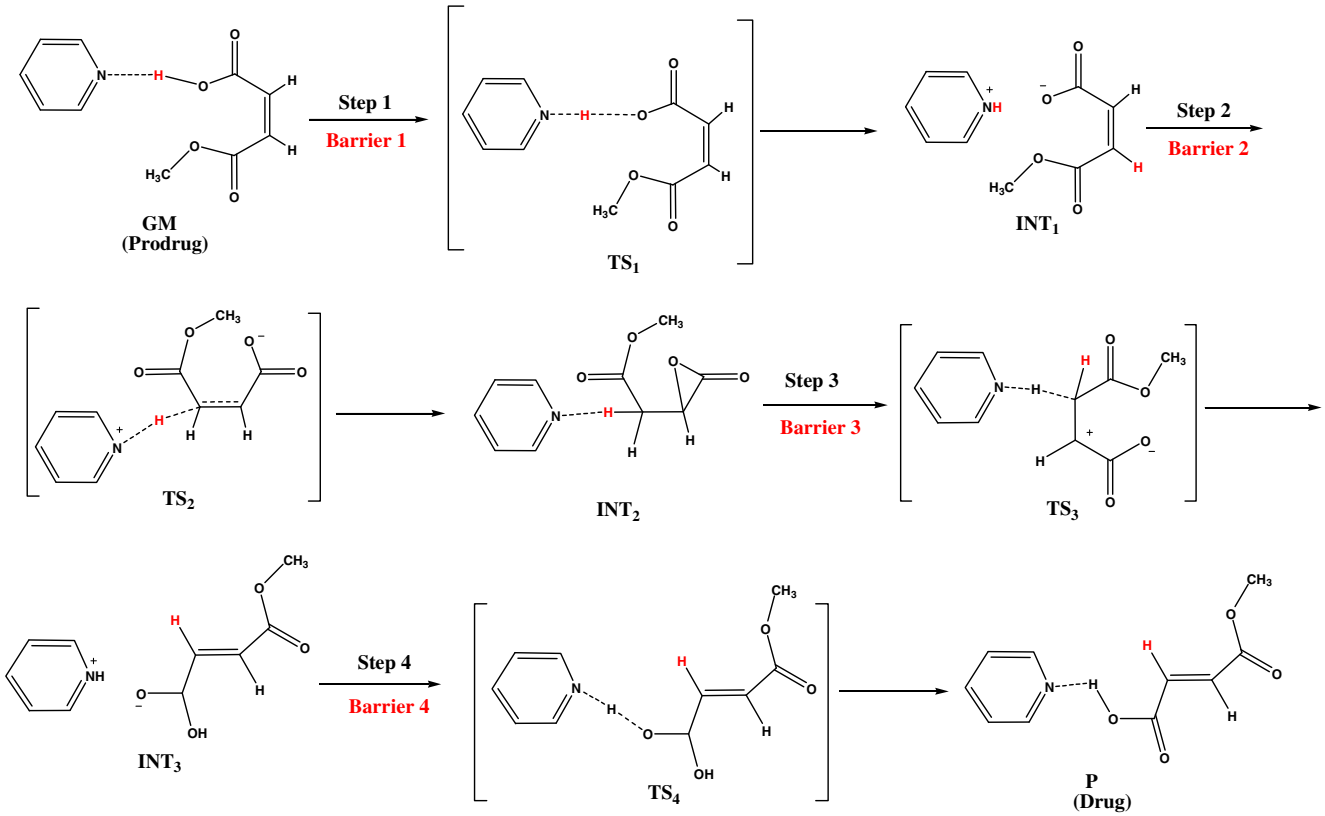

Scheme 2 Mechanistic pathway for the substituted pyridine-catalyzed isomerization of monomethylmaleate into monomethylfumarate. Pyridine was chosen to represent the various pyridine derivatives

the identification of the most stable conformation (global minimum rather than local minimum) for each of the monomethylmaleate pyridine derivative adducts calculated in this study. This was done by 36 rotations of the carboxyl group of the monomethylmaleate moiety about the C6–C7 bond in increments of 10° (i.e., variation of the dihedral angle O8/C7/C6/C5, see Chart 1) and 36 rotations of the methylcarboxyate group about the C4–C5 bond in increments of 10° (i.e., variation of the dihedral angle O3/C4/C5/C6, see Chart 1) and calculation of the energies of the resulting conformers.

Two types of conformations were considered in DFT calculations of the isomerization of monomethylmaleate with a pyridine derivative: one in which the two carbonyl groups are perpendicular each to other (Chart 1a) and another in which they are about 180° each to other (Chart 1b). It was found that the global minimum structures exhibit conformation by which the two carbonyl groups exist at about the same plane (180°) of each other (Chart 1b). In addition, the calculation results demonstrated that the monomethylmaleate moiety exists in a conformation by which the hydroxyl proton of its carboxyl group (H10) is engaged in a hydrogen bonding with a molecule of the pyridine derivative via its amine nitrogen (N11), and the carboxylic group carbonyl oxygen (O9) hydrogen bonds with the α proton of the pyridine derivative (H13) (Chart 1b).

Thermodynamic calculations for the isomerization equilibrium between monomethylmaleate (prodrug) and monomethylfumarate (drug) in the presence of a pyridine derivative

As mentioned in the Introduction, Tocher's team studied the crystals formed from pyridine and 4-dimethylaminopyridine with maleic, fumaric, phthalic, isophthalic, or terephthalic acids by X-ray diffraction [27]. The latter study revealed that the two-component solid forms involving pyridine included both salts and co-crystals, while 4-dimethylaminopyridine crystallized exclusively as a salt, in accordance with the pK_a value of the base catalyst. Furthermore, the study demonstrated that a base-catalyzed isomerization of maleic acid into fumaric acid was obtained in co-crystallization experiments when the base used was pyridine. On the other hand, Rao's team [26] documented that a co-crystalization of maleic acid with 4,4′-bipyridine in apolar solvents gave a 2:1 adduct (two molecules of maleic acid attached to one molecule of a base) where maleic acid was preserved in the cis conformation, whereas, when a polar solvent was used, a 1:1 adduct (one molecule of maleic acid attached to one molecule of the base), by which maleic acid underwent isomerization into formic acid, was observed. The combined results of the two groups demonstrated that the

Chart 1 Schematic representation of the reactants in the substituted pyridine-catalyzed isomerization of monomethylmaleate into monomethylfumarate

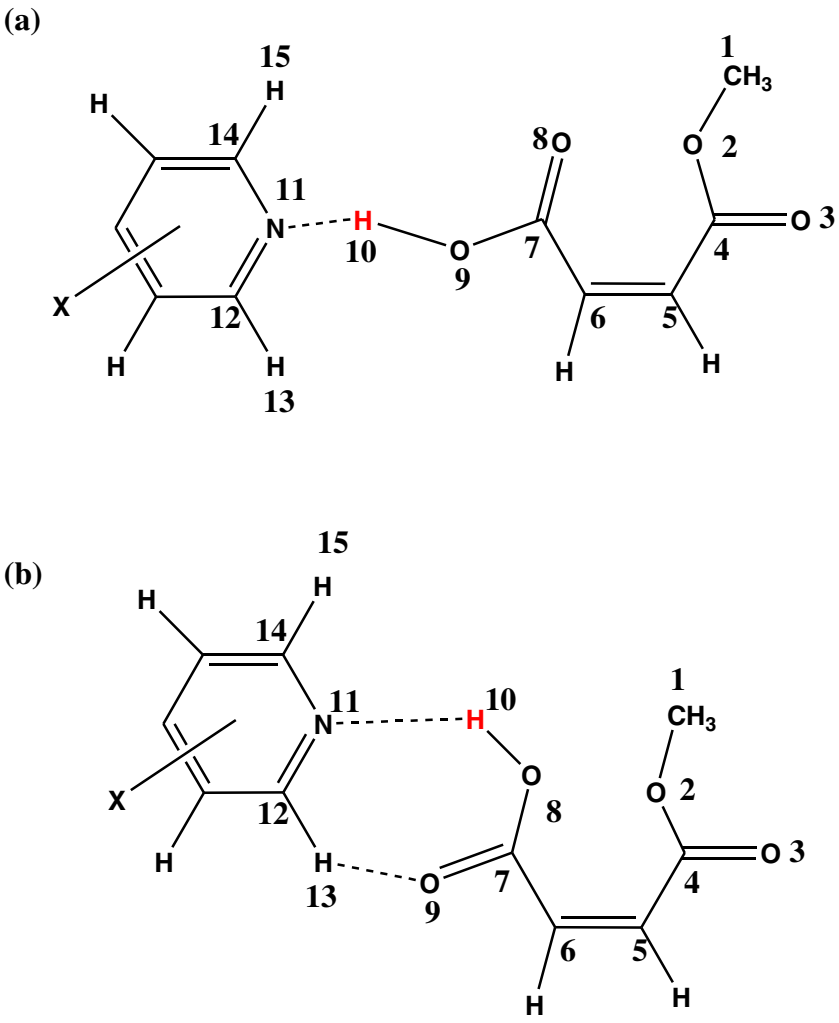

1: X = H
2: X = $N(CH_3)_2$
3: X = o-Cl
4: X = m-Cl
5: X = o-F
6: X = o-Me

equilibrium forming the isomerized product depends strongly on the polarity of the solvent, and the difference in the free energy between the reactants (cis form) and products (trans form). Similarly to the importance of hydrogen bonding in the stabilization of ground state structures, Han's group has showed recently [55–57] that hydrogen bonding in the electronic excited state in several photochemical and photophysical processes, plays an important role in the mode and the dynamics of these processes. Thus, in order to assure complete conversion of monomethylmaleate (prodrug) into monomethylfumarate (drug) it will be necessary to use both an appropriate polar solvent and a base catalyst such that the activation energy of the isomerization reaction is reduced enough to yield the *trans* isomer (drug). Such a base should have an appropriate pK_a value to enable the formation of isomerized product rather than to terminate in a salt formation step (Scheme 1).

Figure 1(a, b) illustrates the DFT at B3LYP/6-31 G (d,p) and B3LYP/6-311+G(d,p) levels optimized structures for

Fig. 1 **a** Density functional theory (DFT) optimizes structures for **1GM–6GM** (**1Cis–6Cis**, **ProD 1–6**). **b** DFT optimizes structures for **1TS2–6TS2**. **c** DFT optimizes structures for **1P - 6P (1Trans Drug–6Trans Drug)** ▶

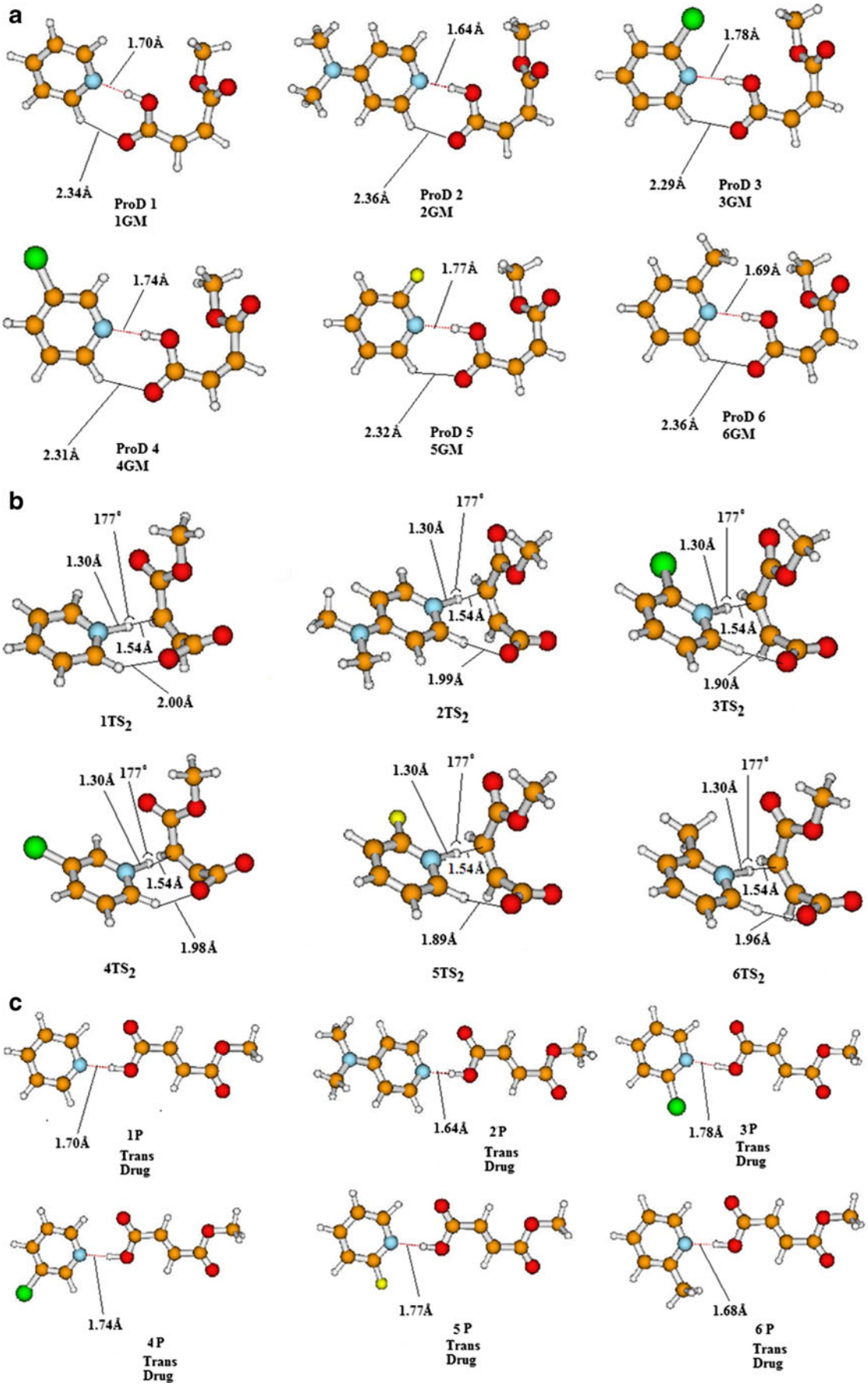
a
1.70Å
2.34Å
ProD 1
1GM
1.64Å
2.36Å
ProD 2
2GM
1.78Å
2.29Å
ProD 3
3GM
1.74Å
2.31Å
ProD 4
4GM
1.77Å
2.32Å
ProD 5
5GM
1.69Å
2.36Å
ProD 6
6GM
b
177°
1.30Å
1.54Å
2.00Å
1TS2
177°
1.30Å
1.54Å
1.99Å
2TS2
177°
1.30Å
1.54Å
1.90Å
3TS2
1.30Å
177°
1.54Å
1.98Å
4TS2
1.30Å
177°
1.54Å
1.89Å
5TS2
177°
1.30Å
1.54Å
1.96Å
6TS2
c
1.70Å
1P
Trans
Drug
1.64Å
2P
Trans
Drug
1.78Å
3P
Trans
Drug
1.74Å
4P
Trans
Drug
1.77Å
5 P
Trans
Drug
1.68Å
6 P
Trans
Drug

the GM structures **1GM-6GM** (prodrug) and the isomerization products from monomethylmaleate **1P-6P** (trans drug). Inspection of Fig. 1(a, h) demonstrates that the reactant and product adducts are stabilized by hydrogen bonding between the pyridine derivative nitrogen and the carboxyl group of the cis or trans isomers. The hydrogen bond lengths in the cis (prodrug) and trans (drug) are quite similar (1.64–1.78 Å). Table 1 lists the free energy values ($\Delta G°=G°_{trans} - G°_{cis}$) for adducts **1**–**6** (Scheme 1) as calculated in the gas phase, DMSO, acetone, methanol and water. Examination of Table 1 reveals that the free energy value for the equilibrium reaction ($G°_{trans} - G°_{cis}$) is not affected significantly by the nature of the solvent except in the case of process **5**.

The solvent effect is relatively profound when the calculated free energies in water and the gas phase are compared. For example, the calculated B3LYP/6-31 G(d, p) ΔG° value for process **1** (Scheme 1) in the gas phase was −6.08 kcal mol^{-1} whereas the value as calculated in water was −4.98 kcal mol^{-1}. Similar trend of the solvent effect on $\Delta G°$ was observed in the calculation results obtained by B3LYP/6-311+G(d,p). On average, the solvent energy contribution was about 1–1.5 kcal mol^{-1} as calculated in both levels. The only exceptional case is process 5, in which the difference in free energy between the values calculated in a solvent such as water and the gas phase was about 3.3 kcal mol^{-1}. This might be attributed to stronger solvation interactions in the cis isomer as compared to that in the trans. Examination of Table 1 reveals that the values of $\Delta G°$ in processes **1**–**6** are quite similar. Therefore, the pK_a or the basicity of the pyridine derivative does not have significant effect on the equilibrium of the prodrug and the drug. The combined results indicate that the drug is thermodynamically more stable than the corresponding prodrug and the effect of the solvent is not dominant.

Kinetic calculations (mechanistic investigation) for the isomerization reaction of monomethylmaleate (prodrug) into monomethylfumarate (drug) in the presence of a pyridine derivative

Scheme 2 illustrates the proposed mechanism for the isomerization of the prodrug monomethylmaleate to its trans isomer, the parental drug. All entities involved in the proposed mechanism were calculated using DFT at B3LYP/6-31 G (d,p) and B3LYP/6-311+ G(d,p) levels of theory. The calculations were done in the gas phase (dielectric constant=1.0), chloroform (dielectric constant=4.9), DMSO (dielectric constant=46.7), methanol (dielectric constant= 32.63), acetone (dielectric constant=20.7), and water (dielectric constant=78.39). Using the calculated DFT values for the energies of the GM structures , **1GM-6GM**, (prodrug, Scheme 2) and the four different transition states (TS1, TS2, TS3 and TS4 for **1**–**6**, Scheme 2) listed in Table S1, the enthalpy activation energies ($\Delta H^{\ddagger}$), entropy activation energies ($T\Delta S^{\ddagger}$), and free activation energies ($\Delta G^{\ddagger}$) for all steps (Scheme 2) were calculated and are tabulated in Table 2. The energy profiles for the isomerization of process **1** as calculated in water, DMSO, MeOH, acetone and the gas phase are shown in Fig. 2. Careful inspection of the data summarized in Table 2 reveals that the rate-limiting step for the isomerization of monomethylmaleate in the presence of a substituted pyridine is the one by which a pyridinium derivative molecule behaves as an acid and adds a proton to the C=C double bond of INT1 (step 2, barrier 2 in Scheme 2). On the other hand, the DFT calculations for step 3 (barrier 3 in Scheme 2) in which a substituted pyridine molecule behaves as a base and abstracts a proton, indicate that the energy barrier for this step is lower than that for step 2. However, the difference between the two barriers, barriers 2 and 3, is dependent largely on the reaction solvent.

Table 1 Density functional theory (DFT) calculated thermodynamic properties for the equilibrium reaction of monomethylmaleate with substituted-pyridine. *Cis* and *trans* refer to prodrug and drug, respectively. *DMSO* Dimethylsulfoxide

Solvent	$\Delta G°$ (trans–cis)[a] 1	$\Delta G°$ (trans–cis) 2	$\Delta G°$ (trans–cis) 3	$\Delta G°$ (trans–cis) 4	$\Delta G°$ (trans–cis) 5	$\Delta G°$ (trans–cis) 6	Dielectric constant
GP/B3L[b]	−6.08	−6.93	−5.93	−6.16	−5.93	−6.35	1
GP/B3L311	−6.09	−5.48	———	———	−5.66	———	
Water/B3L	−4.98	−5.39	−4.80	−5.01	−2.65	−5.12	78.39
Water/B3L311	−4.71	−3.71	———	———	−4.39	———	
DMSO/B3L	−5.01	−5.34	−4.82	−5.04	−2.50	−5.15	46.70
Acetone/B3L	−5.09	−5.47	−4.91	−5.13	−2.05	−5.24	20.70
Methanol/B3L	−5.04	−5.39	−4.85	−5.07	−2.34	−5.18	32.63

[a] GP and $\Delta G°$ refer to gas phase and free activation energy difference in kcal mol^{-1}, respectively

[b] B3L and B3L311 refer to calculated by DFT at B3LYP/6-31 G(d,p) and B3LYP/6-311+G(d,p) levels, respectively.

Table 2 DFT (B3LYP) calculated kinetic and thermodynamic properties for processes **1**–**6**. B3LYP refers to values calculated by B3LYP/6-31 G(d, p) method. $\Delta H^{\ddagger}$ and $\Delta G^{\ddagger}$ are the calculated activation enthalpy and free activation energies (kcal mol^{-1}), respectively

System	pk_a [58]	GP $\Delta H^{\ddagger}$ Barrier 1[a]	GP $\Delta G^{\ddagger}$ Barrier 1	GP $\Delta H^{\ddagger}$ Barrier 2[b]	GP $\Delta G^{\ddagger}$ Barrier 2	H_2O $\Delta H^{\ddagger}$ Barrier 2	H_2O $\Delta G^{\ddagger}$ Barrier 2	GP $\Delta H^{\ddagger}$ Barrier 3[c]	GP $\Delta G^{\ddagger}$ Barrier 3	GP/$\Delta H°$ trans-cis (GM)	GP/$\Delta G°$ trans- cis (GM)
1	5.17	7.17	8.49	49.61	50.8	34.89	36.08	45.23	46.74	−6.39	−6.08
2	9.7	5.89	6.98	45.15	46.24	29.17	30.26	42.69	45.3	−6.97	−6.93
3	0.72	8.66	10.23	53.64	55.29	37.97	39.63	50.38	52.26	−6.23	−5.93
4	2.84	7.85	9.28	51.69	53.01	36.52	37.84	52.22	55.76	−6.33	−6.16
5	−0.44	8.71	10.2	54.01	54.85	37.25	38.09	50.36	51.79	−6.27	−5.93
6	5.97	6.79	8.17	47.48	51.02	31.53	35.07	44.54	46.92	6.44	−6.35

[a] Barrier 1 refers to the process by which a proton is transferred from the maleate moiety into the substituted pyridine

[b] Barrier 2 refers to the step by which INT2 is formed

[c] Barrier 3 refers to that in which INT3 is obtained (see Scheme 2)

Conformational analysis of the entities involved in substituted pyridine-catalyzed isomerization of monomethylmaleate

Starting geometries (GM, Prodrugs, Cis)

Figure 1a illustrates the DFT optimized geometries for the GM structures of the reactants in the isomerization processes of monomethylmaleate into monomethylfumarate in the presence of a pyridine derivative (**1Cis-6Cis**) and Table S1 lists their calculated energies. Inspection of Fig. 1a indicates that the monomethylmaleate moiety exists in a conformation by which its carboxyl group is engaged intermolecularly in two hydrogen bonds with the pyridine derivative nitrogen and hydrogen.

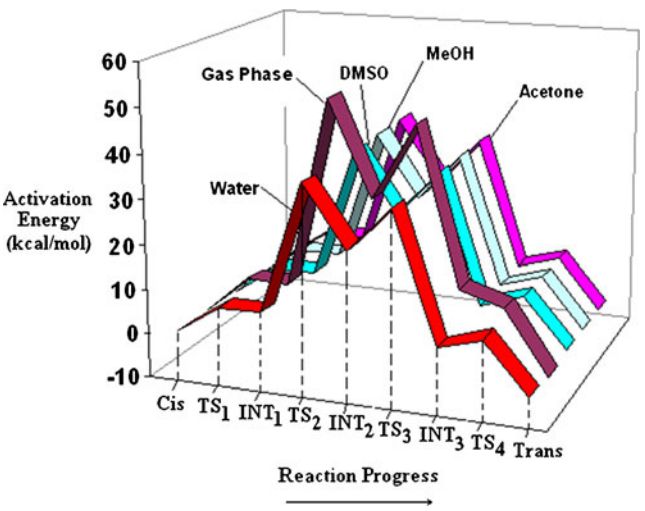

Fig. 2 B3LYP/6-31 G (d,p) calculated energy profiles for the isomerization of monomethylmaleate with pyridine (process **1**) in the presence of water, dimethylsulfoxide (DMSO), methanol (MeOH), acetone and the gas phase

Transition state TS_1

The DFT-calculated optimized structures with selected bond distances and angles for the first transition state (TS_1) in the isomerization of monomethylmaleate in the presence of a pyridine derivative (**1TS1-6TS1**) are summarized in Table S1 and are shown in Fig. S1a.

Intermediate INT_1

The calculated DFT structures for INT1 in the isomerization of monomethylmaleate in the presence of a pyridine derivative (**1INT1-6INT1**) are shown in Fig. S1b and their properties are listed in Table S1. Inspection of the geometries in Fig. S1b demonstrates that INT1 exists as an ion pair composed of the maleate anion and the pyridinuim derivative cation.

Transition state TS_2

The calculated DFT structures for the second transition state (TS_2) in the isomerization of monomethylmaleate in the presence of a pyridine derivative (**1TS2-6TS2**) are listed in Table S1 and are shown in Fig. 1b. Examination of the optimized geometries of the transition states demonstrate that all of them have similar structures. Moreover, Fig. 1b shows that, in addition to the hydrogen bond existing between the pyridinuim proton and the carbon of the C=C double bond, there is a hydrogen bond between the pyridinium H13 and the carboxylate oxygen. The hydrogen bond length H13–O9 was found to lie within in the range 1.89–2.00 Å.

Intermediate INT_2

The calculated DFT geometries for INT2 in the isomerization of monomethylmaleate in the presence of pyridine derivative

as a catalyst (**1INT2-6INT2**) are illustrated in Fig. S1c and their parameters are listed in Table S1. Examination of Fig. S1c demonstrated that the maleate moiety in the intermediate structure underwent cyclization to form an α- lactone ring as a result of intramolecular nucleophilic attack of the carboxylate oxygen anion onto the carbonyl carbon.

Transition state TS_3

The DFT optimized structures for the third transition state (TS_3) in the isomerization of monomethylmaleate in the presence of pyridine derivative as a catalyst (**1TS3-6TS3**) are shown in Table S1 and are illustrated in Fig. S1d. It should be emphasized that the structure of the maleate moiety in **1TS3-6TS3** is quite different from that in **1TS2-6TS2.** The maleate moiety in **1TS2-6TS2** exists in conformation by which the two carboxyl groups are engaged intramolecularly with a hydrogen bonding. This engagement resulted in a cis conformation (Fig. 1b), whereas the conformation of the maleate moiety in **1TS3-6TS3** was the trans orientation (Fig. S1d).

Intermediate INT_3

The calculated DFT optimized structures for INT3 in the isomerization of monomethylmaleate in the presence of a pyridine derivative (**1INT3 - 6INT3**) are shown in Fig. S1e and their energies are listed in Table S1.

Product (Trans Drug)

The DFT optimized geometries for the trans isomers in the isomerization of monomethylmaleate in the presence of pyridine derivative (**1Trans Drug-6Trans Drug**) are depicted in Fig. 1c and their energies are listed in Table S1. Inspection of the calculated geometries in Fig. 1c revealed that **1Trans Drug-6Trans Drug** exhibit conformations by which the carboxyl group is engaged intermolecularly in a hydrogen bond with the pyridine moiety via its hydroxyl proton.

The effect of solvent on the isomerization rate

Inspection of Tables 2 and 3 reveals that the enthalpic and activation energies for steps 2 (barrier 2) in the substituted pyridine-catalyzed isomerization of **1**–**6** are affected greatly by the solvent (dielectric constant). The calculated activation and enthalpic energies in the gas phase (dielectric constant= 1.0) were found to be higher than that calculated in chloroform (dielectric constant=4.9) and the latter were higher than the values calculated in water (dielectric constant=78.39).

Inspection of the activation energy values in Tables 2 indicates that the substituted pyridine-catalyzed cis-trans isomerization of monomethylmaleate is more efficient when the reaction is carried out in a relatively polar solvents, because of enhanced stability of the transition state compared to its corresponding reactants. For example, the gas phase calculated activation energy ($\Delta G^{\ddagger}$) for the isomerization reaction of **1** was 50.80 kcal mol^{-1} while that calculated in water was 36.08 kcal mol^{-1} (Table 3). In fact, when the enthalpic energies for processes **1**–**6** for step 2 (barrier 2, Scheme 2), calculated in different solvents, were examined for correlation with the dielectric constants of the solvents, strong correlations were obtained with a correlation coefficient of $R > 0.98$ (Fig. 3a,b).

It should be noted that when the energy data calculated by B3LYP/6-31 G(d,p) was examined for correlation with that calculated by B3LYP/6-311+ G(d,p), a strong correlation with a correlation coefficient of R=0.99 was obtained.

The effect on isomerization rate of substituted-pyridine pK_a

Examination of the enthalpic energies in Table 2 revealed that substituted pyridine-catalyzed isomerization of **1**–**6** is more efficient when the catalyst used is a strong base (high pK_a). This is because the transition state (TS2 in Scheme 2) is stabilized much more by a strong base due to increased electron donation by a strong base compared to that by a weak base. For example, the calculated activation energy in water for the catalyzed-isomerization by the strong base **2** (pK_a 9.7) is 30.26 kcal mol^{-1} while that catalyzed by a weak base **5** (pK_a −0.44) is 38.09 kcal mol^{-1}. In fact, when the

Table 3 DFT calculated enthalpic energies (kcal mol^{-1}) for substituted pyridine-catalyzed isomerization of monomethylmaleat (**1**–**6**) in different solvents

Solvent	Dielectric constant	$\Delta H^{\ddagger}$ (kcal/mol) 1	$\Delta H^{\ddagger}$ (kcal/mol) 2	$\Delta H^{\ddagger}$ (kcal/mol) 3	$\Delta H^{\ddagger}$ (kcal/mol) 4	$\Delta H^{\ddagger}$ (kcal/mol) 5	$\Delta H^{\ddagger}$ (kcal/mol) 6
Gas phase	1	49.61	45.15	53.64	51.69	54.01	47.48
Water	78.4	34.89	29.17	37.97	36.52	37.25	31.53
Chloroform	4.9	39.29	33.77	42.78	41.17	42.4	36.52
Dimethylsulfoxide	46.7	35.11	29.4	38.21	36.75	37.51	31.79
Acetone	20.7	35.78	30.1	38.96	37.48	38.31	32.56
Methanol	32.4	35.34	26.64	38.47	37.01	37.78	32.05

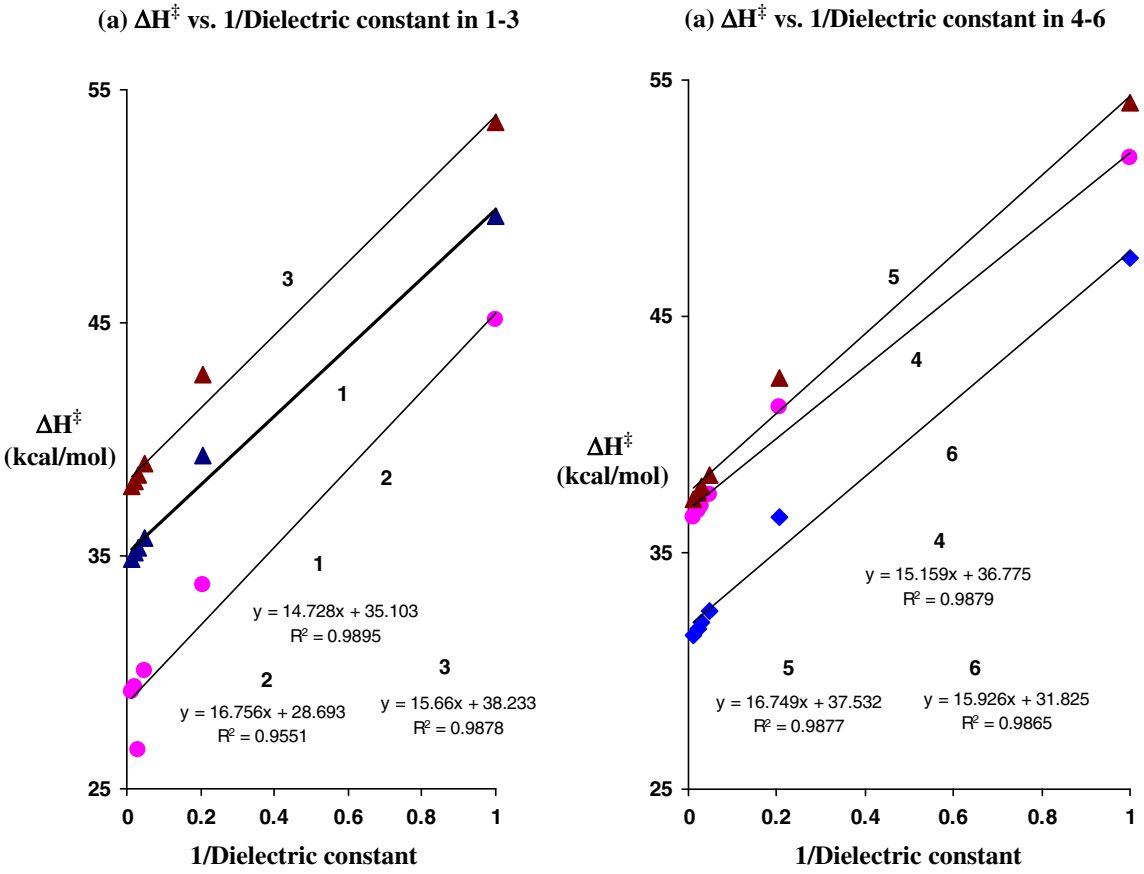

Fig. 3 **a** Enthalpic energy ($\Delta H^{\ddagger}$) in kcal mol^{-1} vs 1/dielectric constant of the solvent in the isomerization of **1**–**3**. **b** Enthalpic energy ($\Delta H^{\ddagger}$) in kcal mol^{-1} vs 1/dielectric constant of the solvent in the isomerization of **4**–**6**

calculated enthalpic energies in the gas phase, water, chloroform, DMSO, acetone and methanol for step 2 (barrier 2, Scheme 2) were examined for correlation with the pK_a values of the substituted pyridine catalyst, strong correlations were obtained with correlation coefficients $R > 0.95$ (Fig. 4a, b). In order to test whether the substituted pyridine catalyst has the same effect on both barriers (barriers 2 and 3), the DFT calculated gas phase enthalpic energies for step 3 (barrier 3, $\Delta H^{\ddagger}$) were correlated with the enthalpic energies for step 2 (barrier 2, $\Delta H^{\ddagger}$). The correlation results illustrated in Fig. 4c indicate good correlation with a correlation coefficient R=0.90. This indicates that the driving force for the approach of the substituted pyridine catalyst (step 2 in Scheme 2) and the proton abstraction by the substituted pyridine (basicity of the catalyst, step 3 in Scheme 2) is the same.

Conclusions and future directions

In summary, we conclude that monomethylmaleate (prodrug) undergoes substituted pyridine-catalyzed isomerization to its trans isomer, the parental drug monomethylfumarate. However, the energy needed for the cis-trans isomerization in water and polar solvents is much lower than that in apolar solvents. The substituted pyridine-catalyzed isomerization proceeds via four steps: (1) a proton transfer from the monomethylmaleate carboxyl groups into the nitrogen of the substituted pyridine to form ion pair INT1; followed by step (2) in which a substituted pyridinum cation moiety approaches the C=C double bond of the maleate moiety to yield INT2; (3) Rotation about the central C–C bond of INT2 followed by proton abstraction by a substituted pyridine molecule to yield unstable INT3; and (4) proton transfer from the substituted pyridinum moiety thus formed into the carboxylate moiety of the fumarate to yield the trans isomer, monomethylfumarate. In addition, the isomerization medium was found to have an large effect on the isomerization rate. Polar solvents, such as water, tend to stabilize transition states TS2 and TS3, and consequently to reduce the activation energy of the process. Moreover, the linear relationship found between the calculated data on one hand and the dielectric constant of the solvent and the pK_a of the catalyst (a substituted pyridine) on the other hand, give a basis from which to evaluate the kinetics of the designed monomethylmaleate prodrugs to be administered into the human

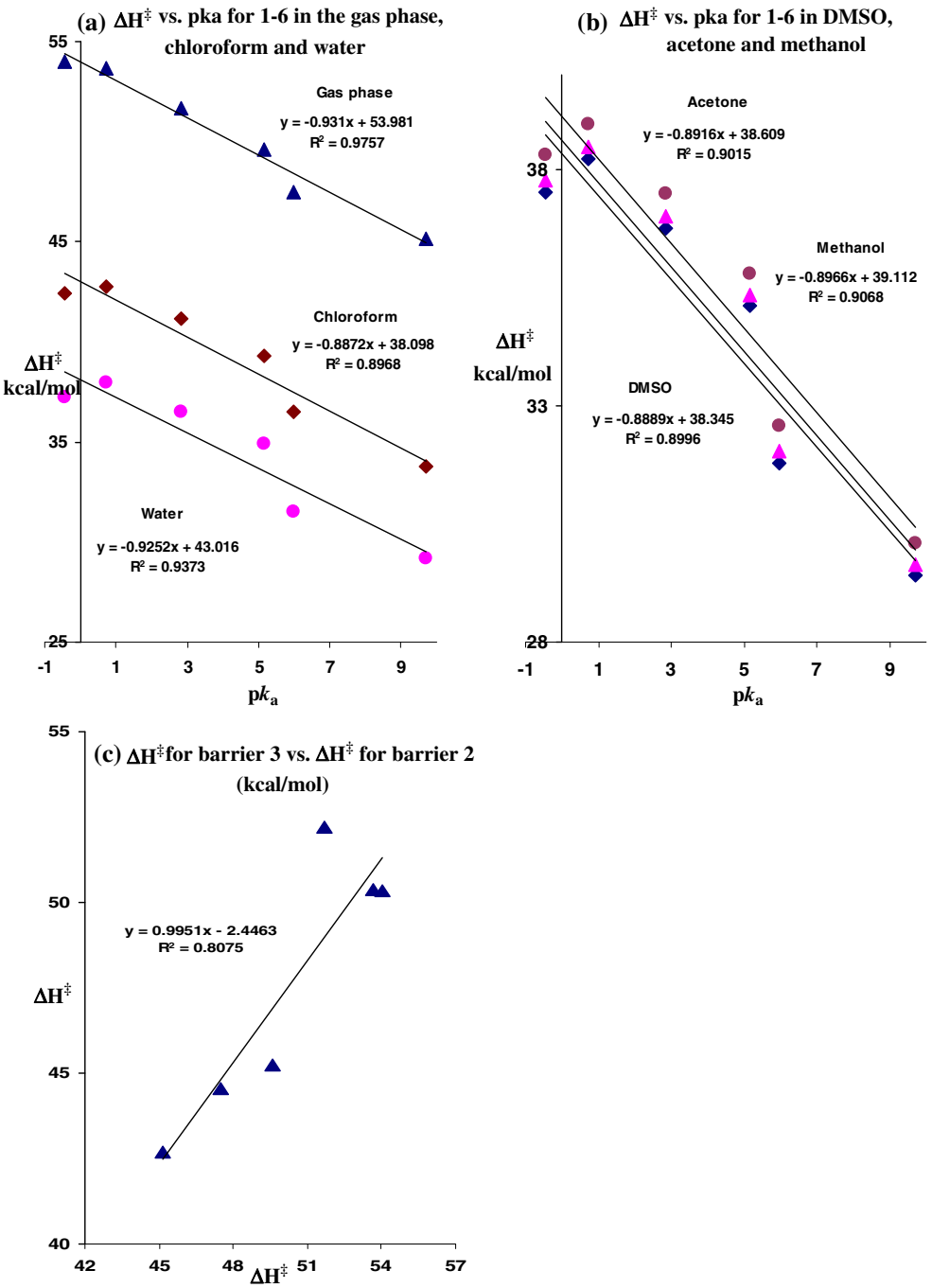

Fig. 4 **a** Enthalpic energy ($\Delta H^{\ddagger}$) in kcal mol^{-1} as calculated in the gas phase, chloroform and water vs pK_a of the catalyst in the isomerization of **1**–**6**. **b** Enthalpic energy ($\Delta H^{\ddagger}$) in kcal mol^{-1} as calculated in DMSO, acetone and methanol vs pK_a of the catalyst in the isomerization of **1**–**6**. **c** Gas phase calculated enthalpic energy ($\Delta H^{\ddagger}$) in kcal mol^{-1} for barrier 3 (TS3) vs gas phase calculated enthalpic energy ($\Delta H^{\ddagger}$) in kcal mol^{-1} for barrier 2 (TS2)

body and to predict the release rate of the parental drug, monomethylfumarate.

Using Arrehnius equation and the water calculation activation energies for the substituted pyridine-catalyzed isomerization listed in Table 2, the relative rates for prodrugs **1**–**6** were calculated using Eqs. 1, 2, 3, 4, and 5,

$$\text{Prodrug relative rate for prodrug } \mathbf{1-6} = k_{\text{prodrug}\mathbf{1-6}}/k_{\text{prodrug}\mathbf{3}} \quad (1)$$

$$\Delta G^{\ddagger}_{\text{prodrug}\mathbf{3}} = -RT \ln k_{\text{prodrug}\mathbf{3}} \quad (2)$$

$$\Delta G^{\ddagger}_{\text{prodrug}\mathbf{1-6}} = -RT \ln k_{\text{prodrug}\mathbf{1-6}} \quad (3)$$

$$\Delta G^{\ddagger}_{\text{prodrug}\mathbf{1-6}} - \Delta G^{\ddagger}_{\text{prodrug}\mathbf{3}} = -RT \ln k_{\text{prodrug}\mathbf{1-6}}/k_{\text{prodrug}\mathbf{3}} \quad (4)$$

$$\text{Prodrug relative rate} = e^{-\left(\Delta G^{\ddagger}_{\text{prodrug}\mathbf{3}} - \Delta G^{\ddagger}_{\text{prodrug}\mathbf{1-6}}\right)/RT} \quad (5)$$

Where T is 298 °K and R is the gas constant.

and their values are as follows: **1** (406.7), **2** (7.6×10^{6}), **3** (1.0), **4** (20.7), **5** (13.5) and **6** (2.2×10^{3}). This result

indicates that the isomerizations of prodrugs **1** and **3**–**5** are expected to be slow, and that of prodrugs **2** and **6** are expected to be relatively fast. Hence, prodrugs **2** and **3**–**5** have the potential to be utilized as prodrugs for slow release of monomethylfumarate in the treatment of psoriasis and multiple sclerosis.

Thus, a strategy for providing desirable prodrugs of fumarates that are capable of being effective in releasing monomethylfumarate in a slow release manner would be as follows: (1) synthesis of monoalkylmaleates by reacting maleic anhydride with the appropriate alcohol in the presence of catalytic amounts of acid [36]; (2) kinetic studies (in vitro) of the synthesized monoalkylmaleates (**ProD 1**–**6**) in the presence of a variety of substituted pyridine derivatives will be performed in physiological environment (37 °C, pH =2.0 and 6.0 in aqueous medium); and (3) for the maleate prodrugs that show slow release in the in vitro studies, in vivo pharmacokinetic studies will be conducted in order to determine the bioavailability and the duration of action of the tested prodrugs. In the light of the in vivo pharmacokinetics, new prodrugs will be design and synthesized.

Acknowledgments The Karaman Co. and the German-Palestinian-Israeli fund agency are thanked for support of our computational facilities. Special thanks are also given to Angi Karaman, Donia Karaman, Rowan Karaman and Nardene Karaman for technical assistance.

References

1. Lohbeck K, Haferkorn H, Fuhrmann W, Fedtke N (2000) Maleic and fumaric acids. In: Ullmann's encyclopedia of industrial chemistry. Wiley-VCH, Weinheim
2. Nieboer C, de Hoop D, Langendijk PNJ, van Diijk E (1989) Systemic therapy with fumaric acid derivates: new possibilities in the treatment of psoriasis. Am Acad Dermatol 20:601–608
3. Mrowietz U, Christophers E (1999) The German fumaric acid ester consensus conference. Br J Dermatol Sep 141(3):424–429
4. Treumer F, Zhu K, Gläser R, Mrowietz U (2003) Dimethylfumarate is a potent inducer of apoptosis in human T cells. J Invest Dermatol 121:1383–1388
5. Litjens NH, van Strijen E, van Gulpen C, Mattie H, van Dissel JT, Thio HB, Nibbering PH (2004) In vitro pharmacokinetics of antipsoriatic fumaric acid esters. BMC Pharmacol 4:22
6. Fachinformation zu Fumaderm® initial/Fumaderm® (1996) Fumedica Arzneimittel GmbH, Heme
7. Naldi L, Rzany B (2002) Chronic plaque psoriasis. Clin Evid 8:688–708
8. Karaman R, Hallak H (2010) Anti-malarial Pro-drugs- a computational aided design. Chem Biol Drug Des 76:350–360
9. Karaman R (2010) Prodrugs of Aza nucleosides based on proton transfer reactions. J Comput Mol Des 24:961–970
10. Karaman R (2011) Computational aided design for dopamine prodrugs based on novel chemical approach. Chem Biol Drug Des 78:853–863
11. Hejaz H, Karaman R, Khamis K (2012) Computer-assisted design for paracetamol masking bitter taste prodrugs. J Mol Model 18: 103–114
12. Karaman R, Dajani KK, Hallak H (2012) Computer-assisted design for atenolol prodrugs for the Use in aqueous formulations. J Mol Model 18:1523–1540
13. Karaman R (2012) Exploring the mechanism for the amine-catalyzed isomerization of dimethyl maleate. A computational study. Tetrahedron Lett 52:6288–6292
14. Clemo GR, Graham B (1930) XXX—The cis-trans ethenoid transformation. J Chem Soc 213–215
15. Nozaki K (1941) cis-trans isomerizations. 11. The mechanism of the amine catalyzed isomerization of diethyl maleate. J Am Chem Soc 63:2681–2683
16. Kodomari M, Sakamoto T, Yoshitomi S (1989) Stereoselective bromination of acetylenes with bromine in the presence of graphite Bull. Chem Soc Jpn 62:4053–4054
17. Baag MM, Kar A, Argade NP (2003) *N*-Bromosuccinimide-dibenzoyl peroxide/azabisisobutyronitrile: a reagent for *Z*- to *E*-alkene isomerization. Tetrahedron 59:6489–6492
18. Rappoport Z, Degani CD, Patal S (1963) Nucleophilic attacks on carbon-carbon double bonds. Part VI.l Amine-catalysed cis-trans-isosmerisation of ethyl a-cyano-p-O-methoxyphenylacrylate through a zupitterionic carbanion in benzene. J Chem Soc 1963: 4513–4520
19. Cook AG, Voges AB, Kammrath AE (2001) Aminal-catalyzed isomerization of and addition to dimethyl maleate. Tetrahedron Lett 42:7349–7352
20. Janus E, Lozynski M, Pernak J (2006) Protic, imidazolium ionic liquids as media for (*Z*)- to (*E*)-alkene isomerization. Chem Lett 35:210–211
21. Trask AV, Motherwell WDS, Jones W (2006) Physical stability enhancement of theophylline via cocrystallization. Int J Pharm 320:114–123
22. Serajuddin ATM, Puddipeddi M (2002) Salt selection strategies. In: Stahl PH, Wermuth CG (eds) Handbook of pharmaceutical salts. VHCA and Wiley-VCH, Weinheim
23. Desiraju GR (2003) Crystal and co-crystal. Cryst Eng Commun 5:466–467
24. Dunitz JD (2003) Crystal and co-crystal: a second opinion. Cryst Eng Commun 5:506–506
25. Aakeroy CB, Salmon DJ (2005) Building co-crystals with molecular sense and supramolecular sensibility. Cryst Eng Commun 7:439–448
26. Chatterjee S, Pedireddi VR, Rao CNR (1998) Unexpected isomerization of maleic acid to fumaric acid on co-crystallization with 4,4′-bipyridine. Tetrahedron Lett 39:2843–2846
27. Mohamed S, Tocher DA, Vickers M, Karamertzanis PG, Price SL (2009) Salt or cocrystal? A new series of crystal structures formed from simple pyridines and carboxylic acids. Crystal Growth Design 9:2881–2889
28. Karaman R (2008) Analysis of Menger's spatiotemporal hypothesis. Tetrahedron Lett 49:5998–6002
29. Karaman R (2009) A new mathematical equation relating activation energy to bond angle and distance: a key for understanding the role of acceleration in the lactonization of the trimethyl lock system. Bioorg Chem 37:11–25
30. Karaman R (2009) Reevaluation of Bruice's proximity orientation. Tetrahedron Lett 50:452–456
31. Karaman R (2009) Accelerations in the lactonization of trimethyl lock systems is due to proximity orientation and not to strain effects. Res Lett Org Chem. doi:10.1155/2009/240253, 5 pages
32. Karaman R (2009) The effective molarity (EM) puzzle in proton transfer reactions. Bioorg Chem 37:106–110
33. Karaman R (2009) Cleavage of Menger's aliphatic amide: a model for peptidase enzyme solely explained by proximity orientation in intramolecular proton transfer. J Mol Struct (THEOCHEM) 910:27–33
34. Karaman R (2009) The *gem*-disubstituent effect-computational study that exposes the relevance of existing theoretical models. Tetrahedron Lett 50:6083–6087

35. Karaman R (2010) Effects of substitution on the effective molarity (EM) for five membered ring-closure reactions- a computational approach. J Mol Struct (THEOCHEM) 939: 69–74
36. Karaman R (2009) Analyzing Kirby's amine olefin – a model for amino-acid ammonia lyases. Tetrahedron Lett 50:7304–7309
37. Karaman R (2010) The effective molarity (EM) puzzle in intramolecular ring-closing reactions. J Mol Struct (THEOCHEM) 940: 70–75
38. Karaman R (2010) The efficiency of proton transfer in Kirby's enzyme model, a computational approach. Tetrahedron Lett 51:2130–2135
39. Karaman R (2010) Proximity vs strain in ring-closing reactions of bifunctional chain molecules—a computational approach. J Mol Phys 108:1723–1730
40. Karaman R (2010) The effective molarity (EM)—a computational approach. Bioorg Chem 38:165–172
41. Karaman R (2010) A general equation correlating intramolecular rates with "attack" parameters distance and angle. Tetrahedron Lett 51:5185–5190
42. Karaman R, Alfalah S (2010) Multi transition states in SN2 intramolecular reactions. Int Rev Biophys Chem 1:14–23
43. Karaman R, Pascal R (2010) A computational analysis of intramolecularity in proton transfer reactions. Org Biomol Chem 8: 5174–5178
44. Becke AD (1993) Density–functional thermochemistry III. The role of exact exchange. J Chem Phys 98:5648–5652
45. Lee C, Yang W, Parr RG (1988) Development of the Colle-Salvetti correlation-energy formula into a functional of the electron density. Phys Rev 37:785–789
46. Stevens PG, Devlin FG, Chablowski CF, Frisch MJ (1994) Ab initio calculation of vibrational absorption and circular dichroism spectra using density functional force fields. J Phys Chem 98: 11623–11627
47. Frisch MJ et al (2009) Gaussian, Revision A.7. Gaussian Inc, Pittsburgh
48. Casewit CJ, Colwell KS, Rappe' AK (1992) Application of a universal force field to main group compounds. J Am Chem Soc 114:10046–10053
49. Murrell JN, Laidler KJ (1968) Symmetries of activated complexes. Trans Faraday Soc 64:371–377
50. Muller K (1890) Reaction paths on multidimensional energy hypersurfaces. Angew Chem Int Ed Engl 19:1–13
51. Cancès MT, Mennucci B, Tomasi J (1997) A new integral equation formalism for the polarizable continuum model: theoretical background and applications to isotropic and anisotropic dielectrics. J Chem Phys 107:3032–3041
52. Mennucci B, Tomasi J (1997) A new approach to the problem of solute's charge distribution and cavity boundaries. J Chem Phys 106:5151
53. Mennucci B, Cancès MT, Tomasi J (1997) Evaluation of solvent effects in isotropic and anisotropic dielectrics and in ionic solutions with a unified integral equation method: Theoretical bases, computational implementation, and numerical applications. J Phys Chem B 101:10506–10517
54. Tomasi J, Mennucci B, Cancès MT (1997) The IEF version of the PCM solvation method: an overview of a new method addressed to study molecular solutes at the QM ab initio level. J Mol Struct (THEOCHEM) 464:211–226
55. Zhao GJ, Han KL (2012) Hydrogen bonding in the electronic excited state. Acc Chem Res 45:404–413
56. Zhao GJ, Liu JY, Zhou LC, Han KL (2007) Site-selective photoinduced electron transfer from alcoholic solvents to chromophores facilitated by hydrogen bonding: a new fluorescence quenching mechanism. J Phys Chem B 111:894–8945
57. Zhao GJ, Han KL (2008) Site-specific salvation of the photoexcited protochlorophyllide a in methanol: Formation of the hydrogen bonded intermediate state induced by hydrogen-bond strengthening. Biophys J 94:38–46
58. Brown HC et al (1955) In: Braude EA, Nachod FC (eds) Determination of organic structures by physical methods. Academic, New York